



ACADÉMIE  
DES SCIENCES  
INSTITUT DE FRANCE

# *Comptes Rendus*

---

## *Chimie*


Briséis Mercadier, Christophe Legein, Mathieu Duttine, Monique Body,  
Ana Gabriela Porras Gutierrez, Sandrine Leclerc, Oleg Lebedev,  
Christian Masquelier and Damien Dambournet

**How mechanochemistry affects the composition and properties of disordered  
fluorite  $\text{BaSnF}_4$ ?**

Volume 27 (2024), p. 343-352

Online since: 27 November 2024

<https://doi.org/10.5802/crchim.361>

 This article is licensed under the  
CREATIVE COMMONS ATTRIBUTION 4.0 INTERNATIONAL LICENSE.  
<http://creativecommons.org/licenses/by/4.0/>



*The Comptes Rendus. Chimie* are a member of the  
Mersenne Center for open scientific publishing  
[www.centre-mersenne.org](http://www.centre-mersenne.org) — e-ISSN : 1878-1543



Research article

# How mechanochemistry affects the composition and properties of disordered fluorite BaSnF<sub>4</sub>?

Briséis Mercadier <sup>a,b,c</sup>, Christophe Legein <sup>Ⓢ,d</sup>, Mathieu Duttine <sup>e</sup>, Monique Body <sup>Ⓢ,d</sup>,  
Ana Gabriela Porras Gutierrez <sup>a,b</sup>, Sandrine Leclerc <sup>a,b</sup>, Oleg Lebedev <sup>f</sup>,  
Christian Masquelier <sup>a,c</sup> and Damien Dambournet <sup>\*,a,b</sup>

<sup>a</sup> Réseau sur le Stockage Electrochimique de l'Energie, RS2E, FR CNRS 3459, 80039 Amiens Cedex, France

<sup>b</sup> Sorbonne Université, CNRS, Physicochimie des Electrolytes et Nanosystèmes Interfaciaux, UMR CNRS 8234, 75005 Paris, France

<sup>c</sup> Laboratoire de Réactivité et de Chimie du Solides, UMR CNRS 7314, 80039 Amiens Cedex, France

<sup>d</sup> Institut des Molécules et Matériaux du Mans (IMMM), UMR 6283 CNRS, Le Mans Université, 72085 Le Mans Cedex 9, France

<sup>e</sup> Institut de Chimie de la Matière Condensée de Bordeaux, ICMCB, UMR 5026, Univ. Bordeaux, CNRS, Bordeaux INP, F-33600 Pessac, France

<sup>f</sup> Laboratoire de Cristallographie et Sciences des Matériaux, CRISMAT, 14000 Caen, France

*E-mail:* damien.dambournet@sorbonne-universite.fr (D. Dambournet)

**Abstract.** Mechanochemistry has been widely used to enable the formation of homogenous mixed phases, particularly in the field of fluoride ion conductors. In this work, we have investigated the effect of applying long duration time of high energy ball milling on the formation of disordered fluorite BaSnF<sub>4</sub>. We have systematically compared the properties of two samples, one prepared using a commonly reported protocol and one obtained after a longer duration. Microstructural analysis obtained by X-ray line refinement and Williamson–Hall diagrams showed that increasing the ball milling time resulted in a decrease in particle size from 13 to 6 nm and suppressed the occurrence of microstrains, which were identified as twinned regions by microscopy analysis. Prolongation of the ball milling treatment is also associated with a decrease in ionic conductivity with identical fluoride ion jump activation energy. <sup>119</sup>Sn Mössbauer spectroscopy revealed the presence of a new signature assigned to Sn(IV) in an oxide–fluoride environment. We hypothesized that this new environment originates from the formation of an anion-excess fluorite-type phase BaSn<sub>1-x</sub>Sn<sub>x</sub><sup>(IV)</sup>F<sub>4</sub>O<sub>x</sub> induced by prolonged milling. Such a hypothesis is supported by the occurrence of fluoride ions located within octahedral sites, which are likely to be bound to Sn(IV) resulting to their lower mobility as shown by <sup>19</sup>F solid-state NMR. Overall, this work demonstrates that the interplay between the microstructure, composition and the transport properties of fluoride ion conductors is indeed complex, with many factors at play, including size, strain, defects or composition.

**Keywords.** Anion-excess fluorite, Interstitial sites, Solid-state electrolyte, Fluoride ion batteries.

**Funding.** French National Research Agency (STORE-EX Labex Project ANR-10-LABX-76-01), Agence Nationale de la Recherche under the France 2030 program (reference 23-PEBA-0002).

*Manuscript received 19 July 2024, revised 3 October 2024, accepted 29 October 2024.*

\*Corresponding author

## 1. Introduction

The use of mechanochemistry for the synthesis of ionic conductors is now a common method applied to compounds with different chemical hardness such as sulfides [1] or fluorides [2]. The reactivity of solid precursors under mechanical forces and local heating is controlled by crystal defects and interphases yielding final compounds with different long-range ordering, i.e., amorphous or crystallized, depending on the phase composition [3]. The reduced crystallite dimension typically found in mechano-synthesized compounds allows for the stabilization of metastable compositions, as exemplified by the solid solution  $\text{BaF}_2\text{-CaF}_2$  with drastic ionic radius mismatch [4]. In addition, mechanochemistry can be further exploited to prepare thermodynamically stable phase with much lower annealing temperature and duration time compared to thermally activated solid-state chemistry [5]. Finally, ball milling treatment has also been used to investigate the effect of crystallite dimensions, microstrains [6,7], or the presence of defects [8] on the transport properties.

In the field of fluoride ion conductors,  $\text{BaSnF}_4$  is a typical example of the beneficial use of mechanochemistry which allows it to produce a disordered structure crystallizing in the  $Fm\bar{3}m$  cubic space group with Ba and Sn occupying the same crystallographic site [9]. This compound has been preliminarily used as a precursor to produce by subsequent annealing [9,10] an ordered related fluorite compound crystallizing in the tetragonal  $P4/nmm$  space group and exhibiting attractive ionic conductivity in the range of  $3.5 \times 10^{-4}$  to  $5 \times 10^{-3} \text{ S}\cdot\text{cm}^{-1}$  at 30 °C [11–13]. In a previous study [14], we investigated the structure and transport properties of this disordered phase and found a fascinating interplay between the Sn(II) lone pair and the fluoride ion dynamics. In the present work, we investigate the effect of a prolonged ball milling treatment on its overall properties. Remarkably, we found that prolonging the duration of the ball milling time not only reduces the particle size but also suppresses defects/microstrains. However, this is accompanied by the formation of an anion-excess fluorite phase containing Sn(IV) and  $\text{O}^{2-}$  anions. This work sheds light on conducting deep structural analysis to understand the reactivity of metal fluoride subjected to mechanochemistry.

## 2. Methods

### 2.1. Ball-milling synthesis

Powder precursors ( $\text{SnF}_2$ , Sigma-Aldrich, 99%;  $\text{BaF}_2$ , Sigma-Aldrich, 99.99%) were weighed and sealed in zirconia milling jars in an argon-filled glove box, with a powder to ball ratio of 1:13. The balls were 10 mm in diameter and made out of zirconia. The precursors were then milled at 400 rotations per minutes for 24 [14] or 99 cycles. Each cycle consisted of 15 min of milling and 15 min of rest to prevent overheating. The samples were labeled as c- $\text{BaSnF}_4$ -24c and c- $\text{BaSnF}_4$ -99c.

### 2.2. Powder X-ray diffraction

Powder X-ray diffraction was performed using a Bruker D8 Advance powder diffractometer, with a copper anode ( $\text{Cu-K}\alpha = 1.5418 \text{ \AA}$ ). The powder XRD pattern was fitted using the Rietveld method as implemented in the Fullprof program, [15] with a split pseudo-Voigt function to model the peaks [16]. The instrumental X-ray line broadening was determined using the  $\text{LaB}_6$  standard sample.

### 2.3. Microscopy

Transmission electron microscopy (TEM) experiments, including electron diffraction (ED), high-angle annular dark-field scanning TEM (HAADF-STEM), and energy-dispersive X-ray (EDX) STEM studies, were performed on a double aberration-corrected JEOL ARM200F cold FEG microscope operated at 200 KV and equipped with a CENTURIO large-angle EDX detector, Orius CCD camera, and a Quantum GIF. The TEM samples were prepared by grinding the materials in an agate mortar in ethanol and depositing the prepared suspension on a Cu-hole carbon grid.

### 2.4. $^{119}\text{Sn}$ Mössbauer spectroscopy

A laboratory-made Halder-type spectrometer with constant acceleration was used for the analysis. It was equipped with a Montana Instruments CryoCore cryogenic system and a  $^{119\text{m}}\text{Sn}$  radioactive source (nominal activity 370 MBq) embedded in a  $\text{CaSnO}_3$  matrix and maintained at room temperature. All spectra were recorded at low temperature (10 K),

with 50 to 70 mg of sample ( $[\text{Sn}] = 5$  to  $8 \text{ mg/cm}^2$ ). The experimental data were analyzed and the  $^{119}\text{Sn}$  Mössbauer hyperfine parameters ( $\delta$ : isomer shift,  $\Delta$ : quadrupole splitting,  $\Gamma$ : full width at half maximum and relative absorption area) were refined using WinNormos<sup>®</sup> software (*Wissenschaftliche Elektronik GmbH*). Isomer shifts are given relative to  $\text{CaSnO}_3$  at room temperature ( $\delta = 0.0 \text{ mm/s}$ ).

### 2.5. Impedance spectroscopy

Electrochemical Impedance spectroscopy was performed on gold-coated  $t\text{-BaSnF}_4$  pellets. Measurements were performed with a BioLogic MTZ-35 impedance analyzer with data collected in the frequency range of  $3.5 \times 10^7 \text{ Hz}$  to  $1 \text{ Hz}$ , under an Ar atmosphere. The compactness of the pellets was approximately 90%.

### 2.6. $^{19}\text{F}$ solid-state NMR

$^{19}\text{F}$  Magic Angle Spinning (MAS) NMR experiments were performed on Bruker Avance III spectrometers operating at  $B_0 = 7.0 \text{ T}$  ( $^{19}\text{F}$  Larmor frequency of  $282.4 \text{ MHz}$ ), using a  $1.3 \text{ mm}$  and a  $2.5 \text{ mm}$  CP-MAS probe head. The  $^{19}\text{F}$  MAS spectra were recorded in direct polarization (single  $90^\circ$  pulse) and using a rotor-synchronized Hahn echo sequence with an interpulse delay equal to one rotor period by default. Unless otherwise noted, the spectra shown were recorded using a Hahn echo sequence. The  $90^\circ$  pulse length and the recycle delay were respectively set to  $1.25 \mu\text{s}$  and  $300 \text{ s}$  for  $c\text{-BaSnF}_4\text{-24c}$ ,  $1.63 \mu\text{s}$  and  $300 \text{ s}$  for  $c\text{-BaSnF}_4\text{-99c}$ ,  $1.25 \mu\text{s}$  and  $900 \text{ s}$  for  $\text{SnF}_2$ ,  $2 \mu\text{s}$  and  $30 \text{ s}$  for  $\text{SnF}_4$  and  $1.5 \mu\text{s}$  and  $300 \text{ s}$  for  $\text{BaF}_2$ . Due to air friction heating, the sample temperature in the  $1.3 \text{ mm}$  probe head varies by up to  $32 \text{ }^\circ\text{C}$  from  $34$  to  $64 \text{ kHz}$ . The isotopic  $^{207}\text{Pb}$  chemical shift of  $\text{Pb}(\text{NO}_3)_2$  was used as the NMR thermometer [17,18].  $^{19}\text{F}$  spectra are referenced to  $\text{CFCl}_3$  and they were fitted by using the DMFit software [19].

## 3. Results and discussion

### 3.1. Microstructural analysis

The mechano-synthesis of  $c\text{-BaSnF}_4$ , reported in the literature results in an X-ray diffraction pattern with typically broad and asymmetric Bragg peaks [9,14].

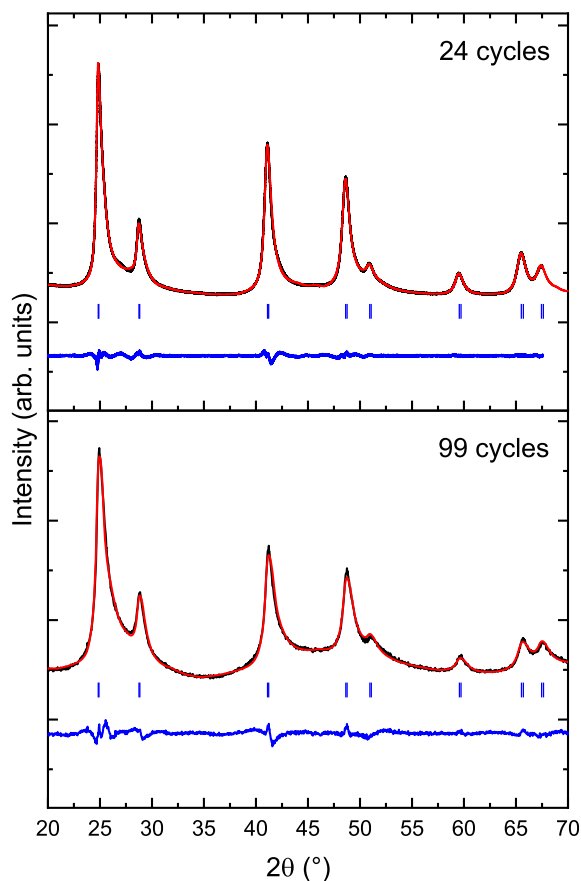


**Figure 1.** Profile matching refinements of  $c\text{-BaSnF}_4\text{-24c}$  and  $c\text{-BaSnF}_4\text{-99c}$ .

An example of the typical diffraction pattern is shown in Figure 1 and refers to a sample prepared by 24 cycles of high energy ball milling, i.e.,  $c\text{-BaSnF}_4\text{-24c}$ . Increasing the mechanical milling time up to 99 cycles, i.e.,  $c\text{-BaSnF}_4\text{-99c}$ , resulted in a significant increase in the broadening of the Bragg peaks (Figure 1). Both samples show close unit cell parameter values of  $6.1964(2)$  and  $6.2039(3) \text{ \AA}$  for 24 and 99 cycles, respectively. To account for the broadening and asymmetry of the Bragg peaks, we performed profile refinement using a split pseudo-Voigt function (see Methods) from which we extracted the position of each peak and the corresponding total integral width ( $\beta$ ).

The origin of the X-ray peak broadening was investigated using the Williamson–Hall (W–H) plot [20] according to the following relation:  $\beta \cos\theta = \lambda/L + 4\varepsilon \sin\theta$  where,  $\lambda$  is the wavelength,  $L$  the average

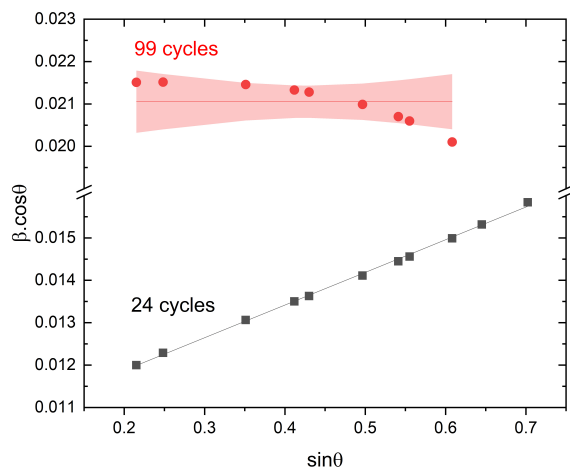


**Figure 2.** Williamson–Hall plots for c-BaSnF<sub>4</sub>-24c and c-BaSnF<sub>4</sub>-99c samples. The pink area refers to a 95% confidence interval.

crystallite size and  $\varepsilon$  the strains. Both the average crystallite size and the strains can be deduced from the intercept and slope of the W–H plot. The W–H plots obtained for both samples are summarized in Figure 2. For c-BaSnF<sub>4</sub>-24c, the plot indicates that the origin of the peak broadening is mainly dominated by strain effects. The deduced average crystallite size is 13 nm. Most noteworthy is the plot obtained for the c-BaSnF<sub>4</sub>-99c sample, which shows that the broadening of the X-ray diffraction peaks originates from a size effect in the absence of strain. It should be noted that for larger  $2\theta$  values, the shape of the peaks is more difficult to capture by the refinement, so that the peaks spread away from a straight line. However, it is clear that the broadening is solely due to a size effect, as confirmed by the average crystallite size value of 6 nm. Overall, the increasing ball-milling time results in a drastic reduction of the particle size by a factor of 2 and seems to suppress the occurrence of strains within the particles.

The presence of strain in c-BaSnF<sub>4</sub>-24c has been previously observed using HRTEM data, where local strain was detected by visible changes in interreticular spacing and the appearance of defects [14]. Further investigations using HAADF-STEM, first confirm that c-BaSnF<sub>4</sub>-24c has a crystallite size of about ten nanometers and that other sources of strain are visible through the presence of twin defects (Figure 3a). Interestingly, c-BaSnF<sub>4</sub>-99c did not show the presence of these twin defects while the crys-

tallite size distribution appears to be narrower and less than ten nanometers (Figure 3b) with well-crystallized aspects. This shows that under mechanical stress, twin defects can act as cleavage planes, reducing both crystallite size and microstrains without implying any recrystallization [21]. In addition, we did not observe any particular changes in the elemental atomic distribution at the particle level (Figure S1).

### 3.2. Sn environments and electron lone pairs

<sup>119</sup>Sn Mössbauer spectroscopy, which probes Sn properties such as the oxidation state, the coordination number and lone pair electrons, was used to investigate how the ball-milling treatment affects these physical properties. The spectra of both samples were reconstructed to extract the hyperfine parameters (Figure 4 and Table 1). The spectrum of c-BaSnF<sub>4</sub>-24c is consistent with previous reports, with two symmetrical quadrupole doublets characteristic of covalently bound Sn(II) and a large quadrupole splitting parameter ( $\Delta > 1.5 \text{ mm}\cdot\text{s}^{-1}$ ) indicating that Sn has a stereochemically active lone pair [22]. These two components (quadrupole doublets) have previously been attributed to different local environments (coordination geometry and bond lengths) for Sn(II) atoms [14]. Prolongation of the ball milling treatment did not affect these environments with similar isomer shift, quadrupole splitting and relative intensity. However, a stronger contribution of Sn(IV) was detected with an isomer shift of  $-0.14 \text{ mm/s}$ . Such a value, intermediate between those of Sn<sup>(IV)</sup>F<sub>4</sub> and Sn<sup>(IV)</sup>O<sub>2</sub> (Figure 4, Table 1) combined with a large quadrupole splitting value (0.72 mm/s), suggests mixed oxide–fluoride and distorted Sn(IV) environments.

### 3.3. Fluoride ion mobility

The influence of the milling time on the ionic conductivity and activation energies was investigated by temperature-dependent electrochemical impedance spectroscopy. The temperature-dependent ionic conductivity shown in Figure 5, exhibits a linear Arrhenius behavior. The activation energy extracted from the Arrhenius plots equals to 0.57 eV in both samples. This shows that increasing the ball milling time does not affect the energy barrier for fluoride

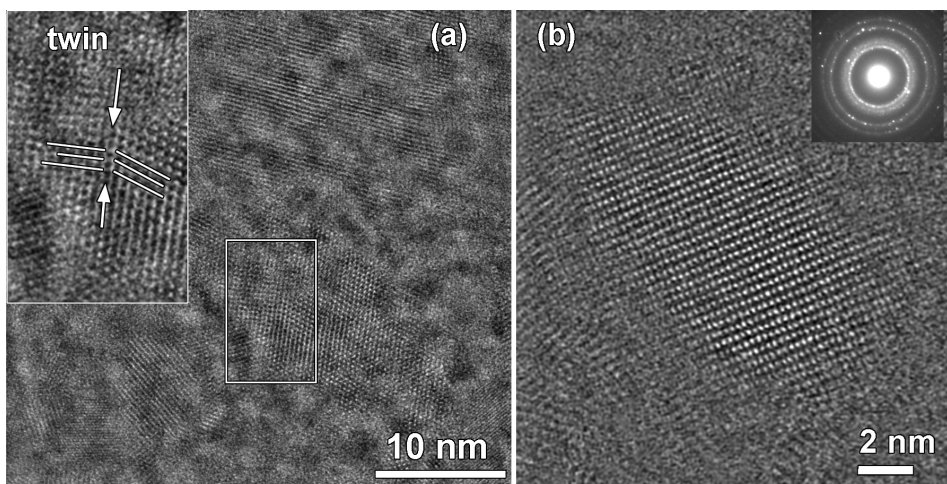


**Figure 3.** HAADF-STEM images from c-BaSnF<sub>4</sub>-24c (a) and c-BaSnF<sub>4</sub>-99c (b).

**Table 1.** Low-temperature (10 K) <sup>119</sup>Sn Mössbauer hyperfine parameters for c-BaSnF<sub>4</sub>-24c and c-BaSnF<sub>4</sub>-99c and reference compounds SnF<sub>4</sub> and SnO<sub>2</sub>

Sample/components	$\delta$ (mm/s)	$\Delta$ (mm/s)	$\Gamma$ (mm/s)	Relative area (%)
c-BaSnF <sub>4</sub> -24c				
Sn(II)-A	3.18(1)	1.81(1)	0.91(1)	55(3)
Sn(II)-B	3.50(1)	1.74(1)	0.93(2)	37(3)
Sn(IV)	-0.14(2)	0.48(6)	0.90(3)	8(3)
c-BaSnF <sub>4</sub> -99c				
Sn(II)-A	3.17(1)	1.78(1)	0.98(3)	46(3)
Sn(II)-B	3.51(2)	1.68(2)	0.96(3)	31(3)
Sn(IV)	-0.11(1)	0.72(2)	0.95(3)	23(3)
SnF <sub>4</sub>	-0.24(1)	0.46(3)	1.07(3)	100
SnO <sub>2</sub>	0.09(1)	0.53(3)	1.06(3)	100

ion jumps. In addition, the ionic conductivity decreases from  $4.60 \times 10^{-6}$  to  $1.58 \times 10^{-6}$  S·cm<sup>-1</sup> at 30 °C when the ball-milling time is extended.

<sup>19</sup>F NMR was used to record the effect of ball-milling duration on the environments and mobility of fluorine. The spectrum of c-BaSnF<sub>4</sub>-24c shows two distinct contributions at -14 ppm and -45 ppm, which are assigned to broad Ba-rich and Sn-rich fluorine environments, based on their proximity to the resonance of BaF<sub>2</sub> ( $\delta_{\text{iso}} = -14$  ppm) and SnF<sub>2</sub> (-44 and -51 ppm), respectively (Figure 6) [14]. In fact, due to fluorine exchange between different sites within the host framework, the rich variety of fluo-

ride ion environments is not observed in the experimental <sup>19</sup>F MAS NMR spectrum. Fluorine exchange on the NMR time scale has been assumed to occur at different rates, between Ba-rich sites, on the one hand, and between Sn-rich sites, on the other hand, each giving rise to a single observed resonance, have been assumed [14].

In c-BaSnF<sub>4</sub>-24c, a third type of fluorine exchange between Ba-rich and Sn-rich environments has been demonstrated using variable-temperature <sup>19</sup>F MAS NMR spectroscopy. As the temperature increases, the relative intensity of the peak assigned to fluoride ions in Sn-rich environments also increases, at

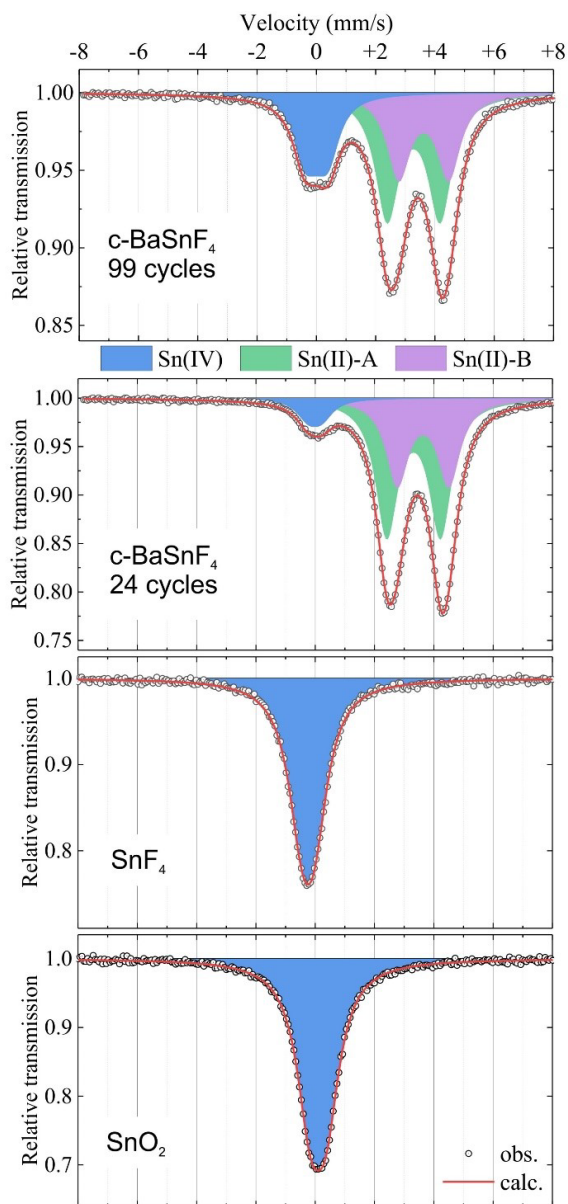


**Figure 4.** Low-temperature (10 K)  $^{119}\text{Sn}$  Mössbauer spectra of  $c\text{-BaSnF}_4\text{-24c}$  and  $c\text{-BaSnF}_4\text{-99c}$  and reference  $\text{SnO}_2$  and  $\text{SnF}_4$ .

the expense of the peak assigned to fluoride ions in Ba-rich environments, confirming some degree of fluoride-ion exchange between Ba-rich and Sn-rich environments [14]. This can also be observed by comparing the  $^{19}\text{F}$  MAS NMR spectra of  $c\text{-BaSnF}_4\text{-24c}$  in Figures 6 and 7, recorded at 64 kHz (at 64 °C due to frictional heating) and 44 kHz (40 °C).

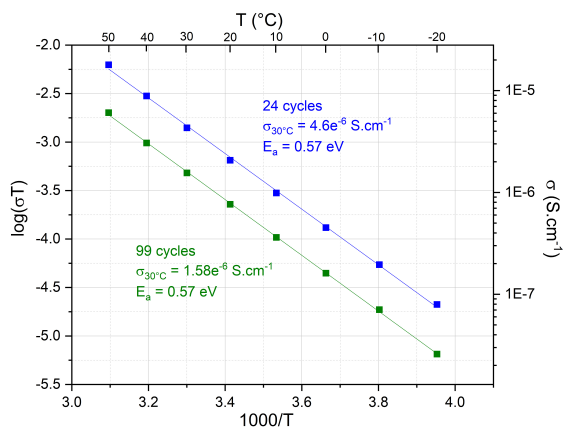


**Figure 5.** Arrhenius plot of the ionic conductivity for  $c\text{-BaSnF}_4$  prepared with 24 and 99 cycles.

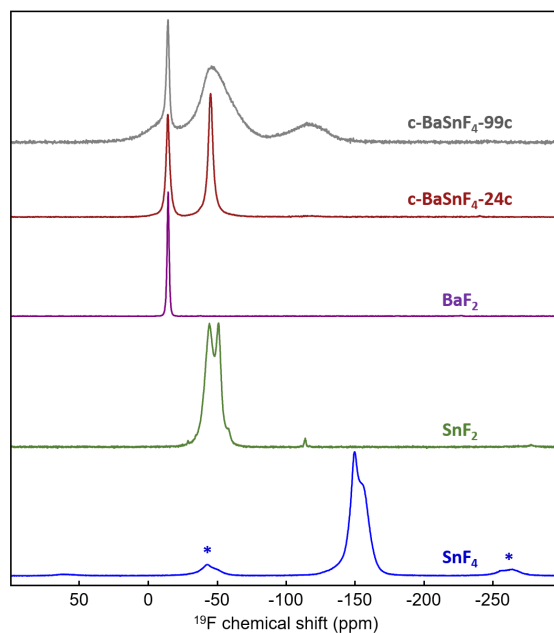


**Figure 6.**  $^{19}\text{F}$  MAS NMR spectra of  $\text{SnF}_4$  (30 kHz),  $\text{SnF}_2$  (64 kHz),  $\text{BaF}_2$  (60 kHz),  $c\text{-BaSnF}_4\text{-24c}$  (64 kHz) and  $c\text{-BaSnF}_4\text{-99c}$  (54 kHz). Fit of the spectra of  $c\text{-BaSnF}_4\text{-24c}$  (64 kHz) and  $c\text{-BaSnF}_4\text{-99c}$  (54 kHz) and characteristics of the lines used for these fits are given as Supplementary Materials (Figures S2 and S3, Tables S1 and S2).

The  $^{19}\text{F}$  MAS NMR spectra of  $c\text{-BaSnF}_4\text{-99c}$  also show these two resonances, with the one assigned to Sn-rich sites being much broader. Moreover, in

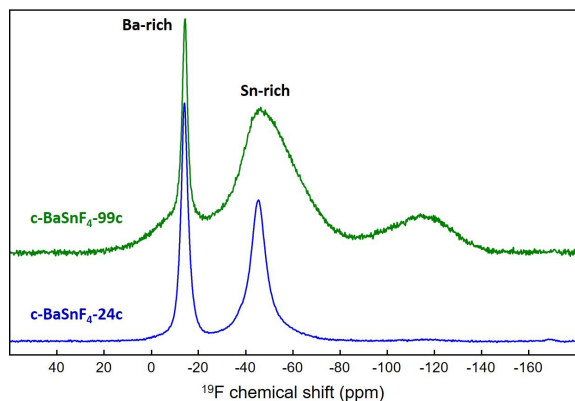


**Figure 7.**  $^{19}\text{F}$  MAS (44 kHz, 40 °C) NMR spectra of  $\text{c-BaSnF}_4\text{-24c}$  (blue) and  $\text{c-BaSnF}_4\text{-99c}$  (green). Fits of these spectra and characteristics of the lines used for these fits are given as Supplementary Materials (Figures S4 and S5, Tables S3 and S4).

contrast to  $\text{c-BaSnF}_4\text{-24c}$ , the relative intensity of this contribution does not increase and its width does not decrease with increasing temperature (Figure 8). Then, for  $\text{c-BaSnF}_4\text{-99c}$ , unlike  $\text{c-BaSnF}_4\text{-24c}$ , motional narrowing of the Sn-rich peak with increasing temperature is not observed, indicating that the so-called fast-exchange regime is not reached and there is no evidence of exchange between Sn-rich and Ba-rich F sites. This results in a lower ionic conductivity.

### 3.4. Environment of $\text{F}^-$ ions from the third contribution of the $^{19}\text{F}$ NMR spectra

In addition to these two main resonances, the spectra of  $\text{c-BaSnF}_4\text{-99c}$  (Figure 6) show at  $\sim -116$  ppm a third broad and less intense resonance. A closer look at the spectra of  $\text{c-BaSnF}_4\text{-24c}$  also shows the presence of this contribution (see Figure 7), at a chemical shift close to  $-115$  ppm, which we did not mention before [14] because of its very low intensity ( $\sim 1\%$ ).

The width of this third contribution indicates a disorder due to the very different environments of the corresponding F-ion sites. In addition, this peak remains almost unchanged with increasing temperature (Figure 8), indicating that these fluoride ions have low mobility.

We have tried to consider the various hypotheses that could explain the origin of this contribution.

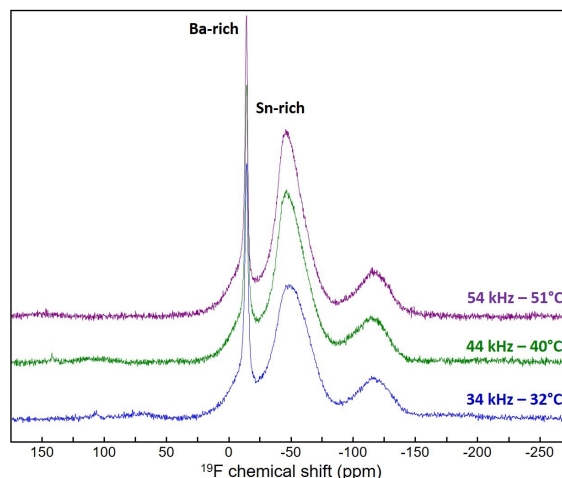


**Figure 8.**  $^{19}\text{F}$  NMR spectra of  $\text{c-BaSnF}_4\text{-99c}$  at various MAS frequencies and temperatures. Fits of these spectra and characteristics of the lines used for the fits are given as Supplementary Materials (Figures S3, S5 and S6 and Tables S2, S4 and S5).

First, such an additional contribution whose average chemical shift is significantly lower than that of the two main resonances, could indicate overcoordinated F-ions (the higher the F-ion coordination number, the lower its  $^{19}\text{F}$  chemical shift [23,24]), i.e., coordination number greater than 4. Indeed, *ab initio* molecular dynamics simulations have revealed, in  $\text{c-BaSnF}_4$ , a complex local structure with a high degree of intrinsic fluoride ion disorder, where 1/3 of the fluoride ions occupy octahedral “interstitial” sites [14]. The detection of resonances characteristic of fluoride ions occupying within these interstitial sites can be explained by the slower exchange in  $\text{c-BaSnF}_4\text{-99c}$  than in  $\text{c-BaSnF}_4\text{-24c}$  (for which the contribution of these sites does not (or almost does not) appear in the spectra). This hypothesis is supported by the observation in the  $^{19}\text{F}$  NMR spectra of the tetragonal phase of  $\text{BaSnF}_4$  of a contribution at a near  $\delta_{\text{iso}}$  value ( $-121$  ppm on average with a maximum at  $-118$  ppm) assigned to  $\text{F}^-$  ions partially occupying the octahedral interstitial sites [25]. The occurrence of F-ions occupying octahedral sites is consistent with the accommodation of Sn(IV) and  $\text{O}^{2-}$  oxide ions in the structure and then with mixed oxide-fluoride and distorted Sn(IV) environments evidenced by Mössbauer.



Using the relative area of the signals assigned to Sn(IV) in Table 1, we evaluated the corresponding formulas, which yielded  $\text{BaSn}_{0.92}^{(\text{II})}\text{Sn}_{0.08}^{(\text{IV})}\text{F}_4\text{O}_{0.08}$  and  $\text{BaSn}_{0.77}^{(\text{II})}\text{Sn}_{0.23}^{(\text{IV})}\text{F}_4\text{O}_{0.23}$  for c-BaSnF<sub>4</sub>-24c and c-BaSnF<sub>4</sub>-99c, respectively. Such anion-excess fluorite-type phase ( $\text{BaSn}_{1-x}^{(\text{II})}\text{Sn}_x^{(\text{IV})}\text{F}_4\text{O}_x$ ) necessarily implies that a part of the anions occupies interstitial positions. Notably, the presence of Sn(IV) and the associated stronger Sn–F bond (along with the absence of lone pair electrons in Sn(IV)) is expected to decrease the mobility of the fluoride ions. Therefore, it can be assumed that the hypothetical fluoride ions located within octahedral sites are partially bound to Sn(IV), reducing their mobility and hence their detection by <sup>19</sup>F NMR.

The second hypothesis concerning the origin of the third contribution in the <sup>19</sup>F NMR spectra is the formation of a Sn(IV) oxide fluoride impurity and Sn(II) depletion in the fluorite. Since it is not detected in the X-ray diffraction patterns (Figure 1), the impurity must be amorphous. Assuming that all Sn(IV) atoms and all oxide ions are involved in the formation of the impurity, its formula would be  $\text{Sn}^{(\text{IV})}\text{OF}_2$  [26] ( $\text{BaSn}^{(\text{II})}\text{F}_4 + (x/2)\text{O}_2 \rightarrow \text{BaSn}^{(\text{II})}\text{F}_{4-2x} + x\text{Sn}^{(\text{IV})}\text{OF}_2$ ) and then the proportion <sup>19</sup>F nuclei involved ( $=2x/4$ ) must be equal to half the proportion of Sn(IV) atoms ( $=x$ ). While the proportions of Sn(IV) can be accurately determined using reconstructions of Mössbauer spectra recorded at low temperature (Table 1), the precise determination of the proportions of F atoms contributing to the third contribution in the <sup>19</sup>F NMR spectra is not guaranteed, since the spin–spin relaxation (transverse relaxation) and subsequent loss of spin coherence is faster for the more mobile F–Sn-rich than for the F–Ba-rich, leading to a loss of intensity of the corresponding NMR signal. Its relative intensity is greater in the spectra recorded with a single pulse rather than a Hahn echo sequence (Figure S7). Single pulse spectra of c-BaSnF<sub>4</sub>-99c and -24c were therefore reconstructed (Figures S8–S9 and Tables S6–S7), allowing us to determine the relative intensities of the third contribution closest to the proportions of involved F atoms.

We can now check whether the fraction of <sup>19</sup>F nuclei involved ( $=2x/4$ ) is equal to half the fraction of Sn(IV) atoms ( $=x$ ). This is the case for c-BaSnF<sub>4</sub>-99c ( $x = 0.23$  (Table 1) and  $2x/4 = 0.122$  (Table S6)), but not at all for BaSnF<sub>4</sub>-24c ( $x = 0.08$  (Table 1) and  $2x/4 = 0.009$  (Table S7)). Thus, in BaSnF<sub>4</sub>-24c,

whether most of the Sn(IV) is not present in the SnOF<sub>2</sub> impurity, or the impurity has a lower F content and therefore a formula of the type  $\text{SnO}_{2-y/2}\text{F}_y$ , which also implies that a fraction, albeit smaller, of the Sn(IV) remains in the fluorite.

Knowledge of the <sup>19</sup>F isotropic chemical shift values of these compounds is required to support or exclude the above hypotheses. Unfortunately, <sup>19</sup>F NMR studies of Sn(IV) oxyfluorides are scarce. In addition to SnOF<sub>2</sub>, which is obtained in amorphous form from  $\text{SnF}_2(\text{ONO}_2)_2$  and is expected to adopt the ReO<sub>3</sub> type structure after crystallization [26], there is  $\text{Sn}_4\text{O}_2\text{F}^{10}$ , a mixed-valence tin oxyfluoride, whose structure has been reported [27], but neither of these compounds appears to have been studied by solid-state NMR. In contrast, more work has been done on fluorine-doped tin oxide ( $\text{SnO}_2:\text{F}$ , FTO), in particular an extensive solid-state NMR study, with a <sup>19</sup>F MAS NMR spectrum showing evidence of a single, relatively broad resonance at  $-113.9$  ppm, which, on the basis of experiments and first-principles quantum-chemical calculations, has been assigned to F atoms occupying O vacancies in  $\text{SnO}_2:\text{F}$  (at 1.2 mol%), i.e., F atoms triple-coordinated to Sn(IV) [28]. Even if the doping rate of the supposed impurity  $\text{SnO}_{2-y/2}\text{F}_y$  is significantly higher, the hypothesis is still convincing. However, if there is an impurity in c-BaSnF<sub>4</sub>-99c, its formula is SnOF<sub>2</sub>, in which the F atoms are doubly coordinated to Sn(IV), while the chemical shifts of <sup>19</sup>F of the third contributions are very close in both samples. Similar <sup>19</sup>F chemical shift values for double and triple coordinated F atoms should exclude the presence of impurities in both samples. However, we lack experimental data on Sn(IV) fluorides and oxyfluorides to completely rule out this hypothesis. In addition, we have observed that the influence of the coordination number of the fluorine through Sn(IV) on its chemical shift is minimal or rare. In fact, in SnF<sub>4</sub>, half of the F atoms are terminal and half are bridging [29], and their chemical shift values, close to  $-150$  ppm, differ by only a few ppm ([30], Figure 6). In contrast, in NbOF<sub>3</sub> and TaOF<sub>3</sub> which adopt the SnF<sub>4</sub>-like structure, the chemical shift values of the terminal and bridging F atoms differ by 200 ppm and 170 ppm, respectively [31].

After outlining various hypotheses, the most plausible is the stabilization of an anion-excess fluorite phase rather than the formation of an impurity. This is supported by microscopic analysis, which

shows that the particles are well crystallized and have a homogenous elemental distribution, while X-ray diffraction does not reveal any impurity. The stabilization of an anion-excess fluorite phase is further supported by Mössbauer spectroscopy and the associated Sn(IV) in mixed oxide–fluoride environments. It is also consistent with the additional resonance observed by  $^{19}\text{F}$  NMR and assigned to fluoride ions located in interstitial octahedral sites. They exhibit low mobility, which may be due to the formation of Sn(IV)–F bonds.

Overall, this work confirms that fluorite is an adaptable framework that can accommodate different cations and anions with deviations from stoichiometry. To determine the stabilization of an anion-excess fluorite phase, the intentional introduction of oxide anions and/or Sn(IV) can be considered. In addition, further characterizations, such as  $^{19}\text{F}$  2D homonuclear correlation spectroscopy, could show that all the fluorine atoms are in the same phase. Finally, a comprehensive study of Sn-based fluoride oxides using  $^{19}\text{F}$  NMR and Mossbauer spectroscopy would be invaluable for a better understanding of the mechanochemistry applied of these compounds.

#### 4. Conclusions

Mechanosynthesis of  $\text{BaF}_2$  and  $\text{SnF}_2$  yields cubic  $\text{BaSnF}_4$ . While short milling times yield the desired product, they also introduce microscopic defects such as strain and twinning regions within the roughly 13 nm crystallites. Interestingly, these defects are suppressed by longer milling times, which also reduce the particle size to 6 nm, suggesting that these twin defects may act as cleavage planes under mechanical stress. The resulting particles are well crystallized and the absence of a second phase has been confirmed by XRD and EDX analysis. However, Mössbauer spectroscopy revealed the presence of Sn(IV) in a disordered mixed oxide–fluoride environment. In addition,  $^{19}\text{F}$  NMR indicated the presence of a peak assigned to fluoride ions located in octahedral sites. We hypothesize that an anion-excess fluorite phase was formed with the general chemical formula  $\text{BaSn}_{1-x}^{(\text{II})}\text{Sn}_x^{(\text{IV})}\text{F}_4\text{O}_x$ . This phase has an overall lower mobility as compared to the stoichiometric compound. Although other parameters such as grain boundaries could be at the origin of the

lower conductivity, the low mobility of fluoride ions located in interstitial sites could be due to bonding with Sn(IV). Overall, this study highlights the complexity of linking the microstructure and transport properties of the material due to the possible influence of other factors such as strain, defects, and even composition.

#### Declaration of interests

The authors do not work for, advise, own shares in, or receive funds from any organization that could benefit from this article, and have declared no affiliations other than their research organizations.

#### Funding

BM, CM, and DD thank the French National Research Agency (STORE-EX Labex Project ANR-10-LABX-76-01) for financial support. DD wishes to thank for support a French government grant managed by the Agence Nationale de la Recherche under the France 2030 program, reference 23-PEBA-0002.

#### Supplementary data

HAADF-STEM images and corresponding EDX elemental mapping of c- $\text{BaSnF}_4$ -99c, experimental and fitted  $^{19}\text{F}$  MAS NMR spectra of c- $\text{BaSnF}_4$ -24c and -99c and features of the NMR lines used in the fits.

Supporting information for this article is available on the journal's website under <https://doi.org/10.5802/crchim.361> or from the author.

#### References

- [1] S. Boulineau, M. Courty, J.-M. Tarascon, V. Viallet, *Solid State Ion.*, 2012, **221**, 1–5.
- [2] A. Düvel, *Dalton Trans.*, 2019, **48**, 859–871.
- [3] A. Banik, T. Famprakis, M. Ghidui, S. Ohno, M. A. Kraft, W. G. Zeier, *Chem. Sci.*, 2021, **12**, 6238–6263.
- [4] A. Düvel, B. Ruprecht, P. Heitjans, M. Wilkening, *J. Phys. Chem. C*, 2011, **115**, 23784–23789.
- [5] A. Düvel, A. Kuhn, L. Robben, M. Wilkening, P. Heitjans, *J. Phys. Chem. C*, 2012, **116**, 15192–15202.
- [6] C. Rongeat, M. A. Reddy, R. Witter, M. Fichtner, *J. Phys. Chem. C*, 2013, **117**, 4943–4950.
- [7] L. N. Patro, K. Hariharan, *Mater. Lett.*, 2012, **80**, 26–28.
- [8] P. Jain, S. Kim, R. E. Youngman, S. Sen, *J. Phys. Chem. Lett.*, 2010, **1**, 1126–1129.
- [9] M. M. Ahmad, Y. Yamane, K. Yamada, *J. Appl. Phys.*, 2009, **106**, article no. 074106.

- [10] F. Preishuber-Pflügl, V. Epp, S. Nakhal, M. Lerch, M. Wilkening, *Phys. Status Solidi C*, 2015, **12**, 10-14.
- [11] F. Fujisaki, K. Mori, M. Yonemura, Y. Ishikawa, T. Kamiyama, T. Otomo, E. Matsubara, T. Fukunaga, *J. Solid State Chem.*, 2017, **253**, 287-293.
- [12] I. Mohammad, R. Witter, M. Fichtner, M. Anji Reddy, *ACS Appl. Energy Mater.*, 2018, **1**, 4766-4775.
- [13] K. Mori, A. Mineshige, T. Emoto *et al.*, *J. Phys. Chem. C*, 2021, **125**, 12568-12577.
- [14] B. Mercadier, S. W. Coles, M. Duttine *et al.*, *J. Am. Chem. Soc.*, 2023, **145**, 23739-23754.
- [15] J. Rodríguez-Carvajal, *Phys. B: Condens. Matter*, 1993, **1-2**, 55-69.
- [16] P. Thompson, D. E. Cox, J. B. Hastings, *J. Appl. Crystallogr.*, 1987, **20**, 79-83.
- [17] A. Bielecki, D. P. Burum, *J. Magn. Reson. A*, 1995, **116**, 215-220.
- [18] L. C. M. Van Gorkom, J. M. Hook, M. B. Logan, J. V. Hanna, R. E. Wasylshen, *Magn. Reson. Chem.*, 1995, **33**, 791-795.
- [19] D. Massiot, F. Fayon, M. Capron *et al.*, *Magn. Reson. Chem.*, 2002, **40**, 70-76.
- [20] G. K. Williamson, W. H. Hall, *Acta Metall.*, 1953, **1**, 22-31.
- [21] A. Düvel, L. M. Morgan, C. V. Chandran, P. Heitjans, D. C. Sayle, *Cryst. Growth Des.*, 2018, **18**, 2093-2099.
- [22] G. Dénès, M. C. Madamba, H. Merazig, A. Muntasar, Z. Zhu, *AIP Conf. Proc.*, 2016, **1781**, article no. 020006.
- [23] M. Biswal, M. Body, C. Legein, A. Sadoc, F. Boucher, *J. Solid State Chem.*, 2013, **207**, 208-217.
- [24] M. Murakami, Y. Noda, K. Takegoshi, *Solid State Nucl. Magn. Reson.*, 2019, **101**, 82-88.
- [25] B. Mercadier, C. Legein, M. Body, T. Famprikis, M. Morcrette, E. Suard, C. Masquelier, D. Dambournet, *Chem. Mater.*, 2024, **36**, 8076-8087.
- [26] K. Dehnicke, *Chem. Ber.*, 1965, **98**, 280-289.
- [27] J.-H. Chang, J. Köhler, *Z. Krist. - New Cryst. Struct.*, 1999, **214**, 147-148.
- [28] Y. S. Avadhut, J. Weber, E. Hammarberg, C. Feldmann, I. Schellenberg, R. Pöttgen, J. Schmedt Auf Der Günne, *Chem. Mater.*, 2011, **23**, 1526-1538.
- [29] M. Bork, R. Hoppe, *Z. Anorg Allg. Chem.*, 1996, **622**, 1557-1563.
- [30] A. T. Kreinbrink, C. D. Sazavsky, J. W. Pyrz, D. G. A. Nelson, R. S. Honkonen, *J. Magn. Reson. (1969)*, 1990, **88**, 267-276.
- [31] O. Zakary, M. Body, T. Charpentier, V. Sarou-Kanian, C. Legein, *Inorg. Chem.*, 2023, **62**, 16627-16640.